HYDROSTATIC DAMPER FOR THE SPACE SHUTTLE MAIN ENGINE (SSME) HIGH PRESSURE OXIDIZER TURBOPUMP (HPOTP)

by David G. Goggin, Joseph K. Scharrer, and Robert F. Beatty

Rocketdyne Division
Rockwell International
6633 Canoga Avenue
Canoga Park, California 91303

ABSTRACT

Alternative methods were evaluated for increasing rotor damping on the SSME HPOTP to reduce bearing dynamic loads and extend their useful life. A unique application of a hydrostatic damper was developed by incorporating a hydrostatic element between stationary turbine bearing support components. Damper design is shown to be dependent on accurate rotordynamic response analysis. Optimization to achieve maximum damper performance under high loading conditions and limited supply flow is discussed. Damping levels approaching critical damping were achieved without major modifications. Bearing dynamic loads are reduced up to 70% and rotor mode logarithmic decrement was increased from 0.085 to as much as 1.0. Possible opportunities for further improvements in damper performance are also discussed.

INTRODUCTION

Hydrostatic bearings have been used as load support devices in many applications since they were invented in 1862 by L. Girard. However, only recently that they have been considered for use as an active damping device. Choy and Halloran[1] used a hydrostatic damper in conjunction with journal and tilting-pad bearings. Their theoretical and experimental results showed that the hydrostatic damper could ensure stable and low-vibration operation for a centrifugal compressor.

Goodwin and Roach[2] presented an experimental and theoretical investigation into the development of a hydrostatic bearing in series with a ball bearing where the dampers' dynamic characteristics could be tuned during rotor operation. Adams and Zahloul[3] presented an analytical study which showed the feasibility and potential benefits of using hydrostatic dampers as active control devices.

Ball bearings used in the SSME HPOTP have suffered wear attributed in part to large dynamic loads[4,5]. It was determined that a fluid film damper should be developed to reduce these loads. The damper would be required to use LOX with its low viscosity as the working fluid; consequently Reynolds' numbers would be high. The state-of-the-art in squeeze film damper technology was reviewed and found to be insufficient to support development of a high Reynolds' number damper. In contrast, hydrostatic bearing technology is well developed and a LOX hydrostatic bearing has been successfully tested by Pratt and Whitney[6].

A project was therefore initiated to develop a so called "hydrostatic damper" for the SSME HPOTP. Preliminary analysis indicated rotor damping could be significantly improved by using the radial clearance between the turbine bearing carrier and its backup support as a hydrostatic bearing. Although the bearing would need to support large static loads imparted by the rotor, risks would be minimized by placing the bearing between nonrotating components.

BACKGROUND

A cross section of the HPOTP is shown in Figure 1. Turbopump operating speeds extend from 19,700 RPM at Minimum Power Level (MPL) to 29,300 RPM at Full Power Level (FPL). Maximum design speed is 30,000 RPM.

The rotor is supported at both ends by duplex angular contact ball bearings. A 0.0005 in. radial clearance, or deadband, is retained between the ball bearing outer race OD and ID of their respective carriers to allow axial movement with the rotor. Additionally, the turbine bearing carrier, referred to as the "cartridge," is supported by a soft axial spring and has a 0.0010 in. radial clearance between it and its backup support for additional axial freedom (Figure 2).

Rotordynamic analysis is performed using rotor and housing finite element models verified through modal testing and integrated using using modal synthesis techniques[4,5,7,8]. Linear critical speeds and stability parameters are summarized in Table 1. Of importance is the 14.7% margin between the maximum design speed and second critical which is less than the 20% margin normally desired. Also of note is the moderate damping available to limit response of the first and second rotor modes.

Rotor unbalance response and the bearing loads experienced during operation are simulated using nonlinear analysis techniques[4,5]. Experience has shown that incorporating nonlinear characteristics such as floating ring seal stick-slip friction and ball bearing nonlinear stiffness and deadband in the analysis is essential for accurately reproducing HPOTP rotordynamic response.

Response predictions from the nonlinear model are correlated to bearing loads measured during engine tests by strain gages located on the pump end bearing carrier. A "test data match" is accomplished using a priori knowledge of sideloads, bearing deadbands, unbalance distributions, and rotor-housing boundary conditions. Bearing package design analysis is then based on the upper envelope of predicted bearing loads.

DESIGN REQUIREMENTS

Radial clearances in the turbine bearing package previously described are necessary to allow axial movement with the rotor. During normal operation, though, static rotor loads exceed dynamic loads such that the rotor operates fully engaged against the bearing carrier and backup support. Rotor orbits do not enter the deadband clearance, avoiding the detrimental effects of "deadband interaction" on rotor response and stability(4).

Figure 3 shows a schematic of the bearing package nonlinear model and proposed location for the hydrostatic damper. The damper is formed by developing a hydrostatic film between the bearing carrier and backup support. The corresponding analytical bearing model included ball bearing deadband, nonlinear stiffness versus deflection, and cartridge-backup support radial clearance. Ability to simulate contact between the bearing package and hydrostatic damper components due to relative motion was retained.

The hydrostatic film is located in series with the bearings and backup support that previously operated fully engaged, thereby reducing the effective rotor-casing support stiffness. A design goal was to ensure the subsequent reduction in margin between maximum operating speed and second critical is offset by a proportionately larger increase in effective rotor damping. Also, although the hydrostatic film is located between nonrotating components, sufficient load capacity was required to avoid contact between damper components.

Accurate nonlinear rotordynamic response analysis proved essential to the damper design effort. By definition the effective increase in rotor damping is dependent on the magnitude of the relative deflections across the damper hydrostatic film. Maximum damping is achieved with relative deflections just less than the available clearance. Accurate response analysis is necessary to ensure the damper is optimized for maximum benefit without allowing contact between component surfaces.

The nonlinear models described were used to determine loads and deflections across each of the bearing/damper package components. Key results are shown

in Figure 4. The potential reduction in turbine bearing load is shown for a range of damper conditions, along with the minimum acceptable stiffness to avoid contact between damper surfaces.

Two phenomena are involved in producing the load reductions shown, one of which can only be predicted by a response analysis incorporating bearing/damper package nonlinear characteristics. For values of hydrostatic film stiffness near the minimum acceptable limit, maximum improvement in rotor damping is achieved minimizing the resulting dynamic bearing loads. At large values of stiffness, though, the hydrostatic film acts as a rigid support between the bearing carrier and backup structure, effectively eliminating the 0.0010 in. radial clearance between them. This clearance has a significant influence on the effective second critical speed and therefore on bearing loads at FPL as shown in Figure 5. Reductions in bearing load shown in Figure 4 for values of film stiffness greater than 6.0 E+06 lb/in are almost exclusively due to this reduction in effective bearing deadband.

Reductions in load due to increased rotor damping are preferable to load reductions via decreased bearing package deadband. The margin between the second critical speed and maximum operating speed, and correspondingly the dynamic bearing loads experienced at FPL, can be adversely affected by pump build tolerances and/or wear during operation. These factors might fully offset predicted reductions in response with a very stiff damper. In contrast, increased rotor damping would limit dynamic response regardless of these factors, producing uniform behavior for a wide range of pump conditions.

This is further illustrated by results from the linear eigenvalue analysis. Figures 6 shows the impact of damper characteristics on second rotor mode logarithmic decrement at FPL. As shown, the largest increase in effective rotor damping is achieved when damper stiffness is just sufficient to avoid bore contact.

Another key aspect of the damper was potential sensitivity to manufacturing tolerances. Preliminary damper designs optimized for nominal dimensions were found to exhibit unacceptable variations in stiffness for the expected range of manufacturing tolerances. Damper coefficients for a typical configuration

varied from 3.1 E+06 to 7.4 E+06 lb/in for a target radial clearance tolerance of 0.0010 - 0.0025 in. As shown in Figure 7, smaller radial clearances also result in larger values of damping as well as stiffness such that the nominal reduction in bearing load appears insensitive to damper operating clearance. As discussed, the predicted load reductions at high values of damper film stiffness would be less consistent than if the damper stiffness remained near the point of optimum damping regardless of manufacturing tolerances. A final design goal was therefore to optimize the damper design to produce nearly uniform film stiffness over the range of expected operating clearances.

DAMPER ANALYSIS

The hydrostatic bearing code used is based on the theory of Artiles, et. al.[9]. This code utilizes Reynolds' equations and accounts for turbulent flow, fluid inertia at the recess edge, and has been extended to account for a tapered bore. This code has been anchored to the available experimental results for hydrostatic bearings in oil[10,11,12,13], water[14,15], liquid hydrogen and liquid oxygen[6], liquid hydrogen[16], and liquid hydrogen and freon[17] and has been found to give reasonable results for leakage, torque, and direct stiffness. There are no reliable results in the literature for cross-coupled stiffness and direct damping.

Rotordynamic analysis determined the limiting design characteristic was damper stiffness. The parasitic nature of the damper supply flow also required that leakage be kept to a minimum. Consequently damper design revolved around optimizing the stiffness/leakage ratio. Parameters to be defined were the number of recesses, area ratio, dimensions of the recess, orifice diameter, recess depth, and radial clearance.

The number of recesses was constrained to a multiple of 3 by the configuration of the 18 bolt hole bearing package support flange which also serves as the damper supply annulus. Nine recesses were determined to provide the optimum balance between stiffness and manufacurability. Stress considerations would not allow the recesses to be located on the damper stator. A novel

configuration was therefore developed with the recesses located on the damper journal as shown in Figure 8.

Preliminary calculations showed a radial clearance of 0.0025 in. or less would be necessary to meet damper stiffness requirements. Figure 9 illustrates the stiffness/leakage ratio as a function of area ratio for the maximum radial clearance of 0.0025 inches. (Area ratio = Total Recess Area/Total Bearing Area.) The figure shows the 0.20 area ratio is optimum for this application. Figure 10 shows the stiffness/leakage ratio as a function of the axial length to circumferential width ratio for the 0.20 area ratio at the maximum radial clearance. The figure shows that a recess with a circumferential width twice the axial length is optimum for this application.

The orifice diameter was optimized according to the well known results in Figure 11. As shown, a pressure ratio of 0.5 yields the optimum combination of stiffness and damping. Testing proved necessary to accurately assess the orifice loss coefficient. Results of this testing are beyond the scope of this paper and will be published at a later date.

Preliminary analysis had shown that optimizing the orifice diameter for nominal damper clearances resulted in a wide variation in stiffnesses for the expected range of manufacturing tolerances. Analysis was performed to determine the effect of optimizing orifice diameter on the minimum, nominal, or maximum radial clearance case. An integrated flowpath/damper analysis was required since variations in damper radial clearance significantly alter the supply flowpath resistance. Figure 12 illustrates dimensionless damper stiffness as a function of radial clearance for the following four cases:

1) The orifices optimized for each clearance
2) The orifices optimized for the nominal clearance
3) The orifices optimized for the minimum clearance
4) The orifices optimized for the maximum clearance

As shown, the minimum variation in stiffness occurs when the orifice is optimized for the maximum radial clearance expected.

Depth of the hydrostatic damper recess was determined using the guidelines from Pratt and Whitney[6] for LOX. It is stated that the pressure variation within the recess should not exceed 10% of the pressure drop and that the ratio of the recess volume to the total volume of the bearing film be less than 2.0 for LOX.

Based on the analyses just described, the final damper configuration was defined as follows:

Number of recesses = 9
Recess dimensions = 0.457 X 0.914 in.
Recess depth: 0.009 < depth < 0.011 in.
Radial clearance: 0.001-0.0025 in.
Orifice diameter = 0.095-0.105 in.

RESULTS

The resulting improvement in rotordynamic characteristics are shown in Table 2 for the range of damper operating conditions. By designing the damper to provide uniform stiffness over the range of operating clearances, consistent performance is achieved. The only variation is in the degree of rotor damping, or in turn, the degree of dynamic bearing load reduction achieved.

The stiffness required to avoid contact results in only a slight loss in margin between maximum operating speed and the second critical. This is more than offset by improved second mode damping. A significant reduction in first critical speed is noted since the hydrostatic film is relatively soft at the lower speeds. The film stiffness increases approximately with the square of the operating speed, so the frequency of the first mode at FPL is not significantly lowered. (It is typically required that the first mode frequency remain greater than 50% of the operating speed). This, along with the increase in first mode damping, indicate there should be no problem with first mode stability. Linear stability analysis indicates both first and second mode stability threshold speeds exceed 50,000 RPM.

As expected from these results, there is a significant reduction in bearing loads at speeds near FPL. Figure 13 shows nominal turbine bearing dynamic loads for speeds ranging from 5,000 to 35,000 RPM. Figures 14 and 15 show reductions in pump and turbine end dynamic bearing loads at FPL. Dynamic loads are reduced from 50% - 65% depending on damper operating clearances.

Damper performance is currently limited to stiffness values greater than those shown in Figure 4 to prevent contact between damper components. If rotor loads are reduced as planned through other pump modifications, latitude would exist to improve damper performance. Engine tests with the damper will therefore be monitored closely to take advantage of potential performance improvements. Reductions in damper stiffness could be easily accomplished through minor adjustments in radial clearance or supply pressure.

Final damper design details are currently near completion. Fabrication and installation of a test damper in a development turbopump is expected during 1989. The turbopump, instrumented with accelerometers and strain gages on the pump end bearing carrier, will then be hot fire tested in simulated flight mission test profiles. Results will be compared against data from previous tests on this redesign pump as well as the data base from other configurations tested.

CONCLUSION

A novel hydrostatic damper configuration was developed for reducing ball bearing dynamic loads on the SSME HPOTP. The necessity for accurate rotordynamic response predictions in determining damper design requirements was illustrated. Damper design optimization was presented, including the benefits of optimizing the orifice diameter for the maximum expected radial clearance to produce uniform damper performance. Damping levels approaching critical damping were achieved without major modifications. Bearing dynamic loads are reduced up to 70% and rotor mode logarithmic decrement was increased from 0.085 to as much as 1.0. Possible opportunities for further improvements in damper performance are also discussed.

REFERENCES

1. Choy, K.C., and Halloran, J.D., "Application of Hydrostatic Squeeze-Film Dampers," ASLE Transactions, Vol. 25, No. 2, pp 245-251, 1982.

2. Goodwin, M. and Roach, M., "Vibration Control in Rotating Machinery Using Variable Dynamic Stiffness Squeeze Films," USGAD-A174433, March 1986.

3. Adams, M.L., and Zahloul, H., "Attenuation of Rotor Vibration Using Controlled-Pressure Hydrostatic Squeeze-Film Dampers," ASME 11th Biennial Conf. on Vibration and Noise, Boston, Mass., 27-30 Sept. 1987.

4. Childs, D.W., and Moyer, D.S., "Vibration Characteristics of the HPOTP (High-Pressure Oxygen Turbopump) of the SSME (Space Shuttle Main Engine)," ASME Paper #84-GT-31, 29th Intl. Gas Turbine Conf., Amsterdam, The Netherlands, 4-7 June 1984.

5. Beatty, R.F., and Hine, M.J., "Load Cell Verification of the Uprated High Pressure Oxygen Turbopump for the Space Shuttle Main Engine," 9th Aerospace Testing Seminar, El Segundo, CA, October 1985.

6. Pratt and Whitney, "Investigation of Hydrostatic Bearings for Use in High Pressure Cryogenic Turbopumps," AFRPL-TR-67-130, May 1967.

7. Glasgow, D.A., and Nelson, H.D., "Stability Analysis of Rotor-Bearing Systems Using Component Mode Synthesis," ASME Journal of Mechanical Design, Vol. 102, No. 2, pp 352-359, April 1980.

8. Nelson, H.D., et. al., "Nonlinear Analysis of Rotor-Bearing Systems Using Component Mode Synthesis," ASME Journal of Eng. for Power, Vol. 105, pp. 606-614, July 1983.

9. Artiles, A., Walowit, J. and Shapiro, W., "Analysis of Hybrid, Fluid Film Journal Bearings with Turbulence and Inertia Effects," Advances in Computer Aided Bearing Design, ASME, 1982, pp25-52.

10. Raimondi and Boyd, "An Analysis of Orifice and Capillary-Compensated Hydrostatic Journal Bearings," Lubr. Eng., 13, 1, Jan. 1957, pp28-37.

11. Ghosh, B., "Load and flow Characteristics of a Capillary Compensated Hydrostatic Journal Bearing," Wear, 23, pp. 377-386, 1973.

12. Ho, Y. and Chen, N., "dynamic Characteristics of a Hydrostatic Journal Bearing," Wear, 63, pp. 13-24, 1980.

13. Chaomleffel, J., "Influences des Forces D'inertie en Lubrification Hybride," Thése de Docteur Ingenieur, Université Claude Bernard, Lyon, 1983.

14. Aerojet, "Hydrostatic Bearing Feasibility Program," AFRPL-TR-65-120, December 1965.

15. Heller, S., "Static and Dynamic Performance of EXternally Pressureized Fluid Film Journal Bearings in the Turbulent Regime," ASME Journ. of Lubr. Tech., July 1974, pp. 381-389.

16. Spica, P., Hannum, N., and Meyer, S., "Evaluation of Hybrid Hydrostatic Bearing for Cryogenic Turbopump Application," NASA TM 87255, April 1986.

17. Butner, M. and Murphy, B., "SSME Long Life Bearings," NASA CR-179455, 1986.

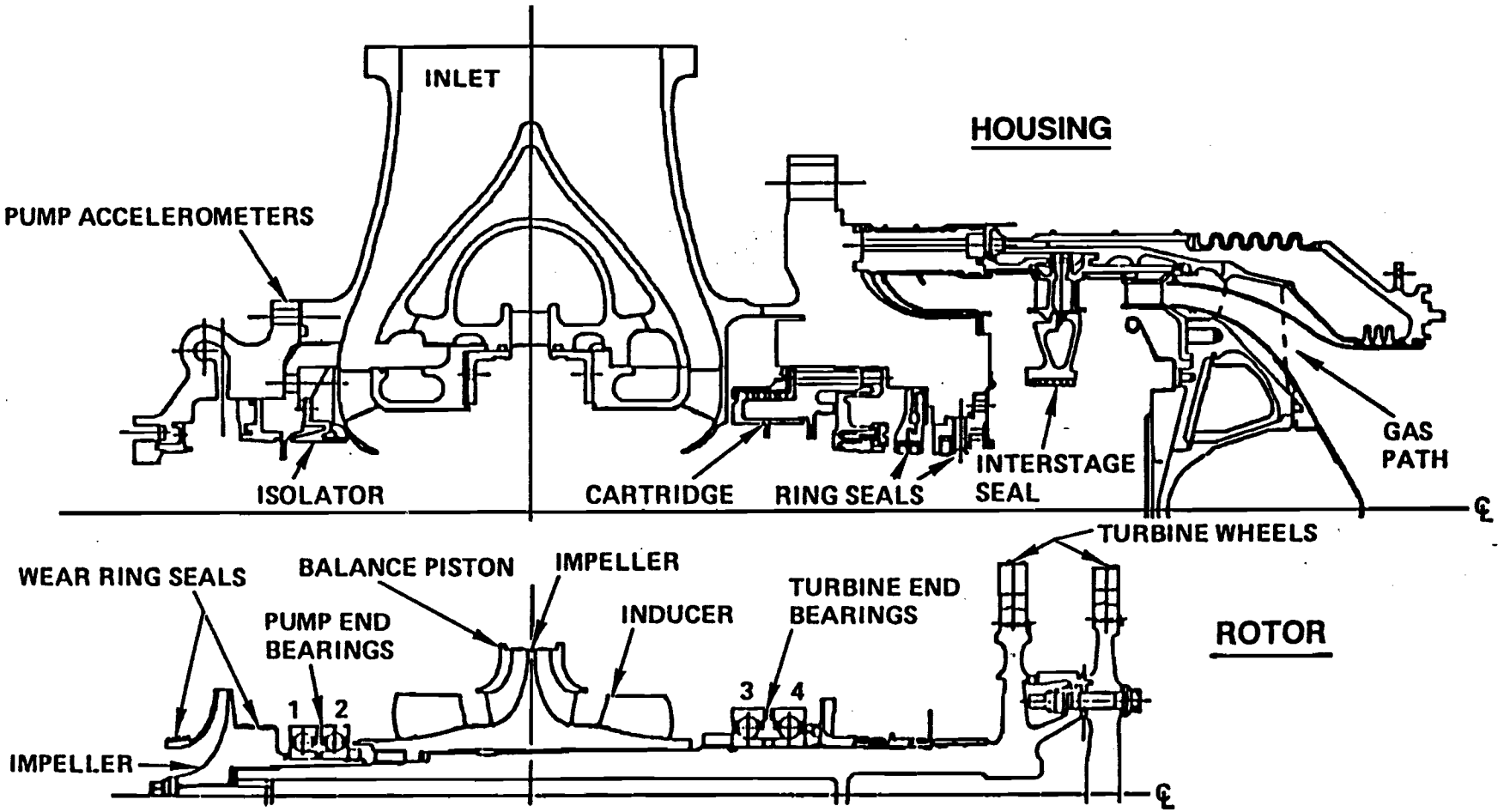

DBC-12

Figure 1. Half Cross Section of High Pressure Oxygen Turbopump

SSME HPOTP TURBINE BEARING PACKAGE

NORMAL OPERATION:
ROTOR FIXED LOADS > DYNAMIC LOADS
BEARING PACKAGE OPERATES FULLY ENGAGED TO ONE SIDE OF DEADBAND CLEARANCE

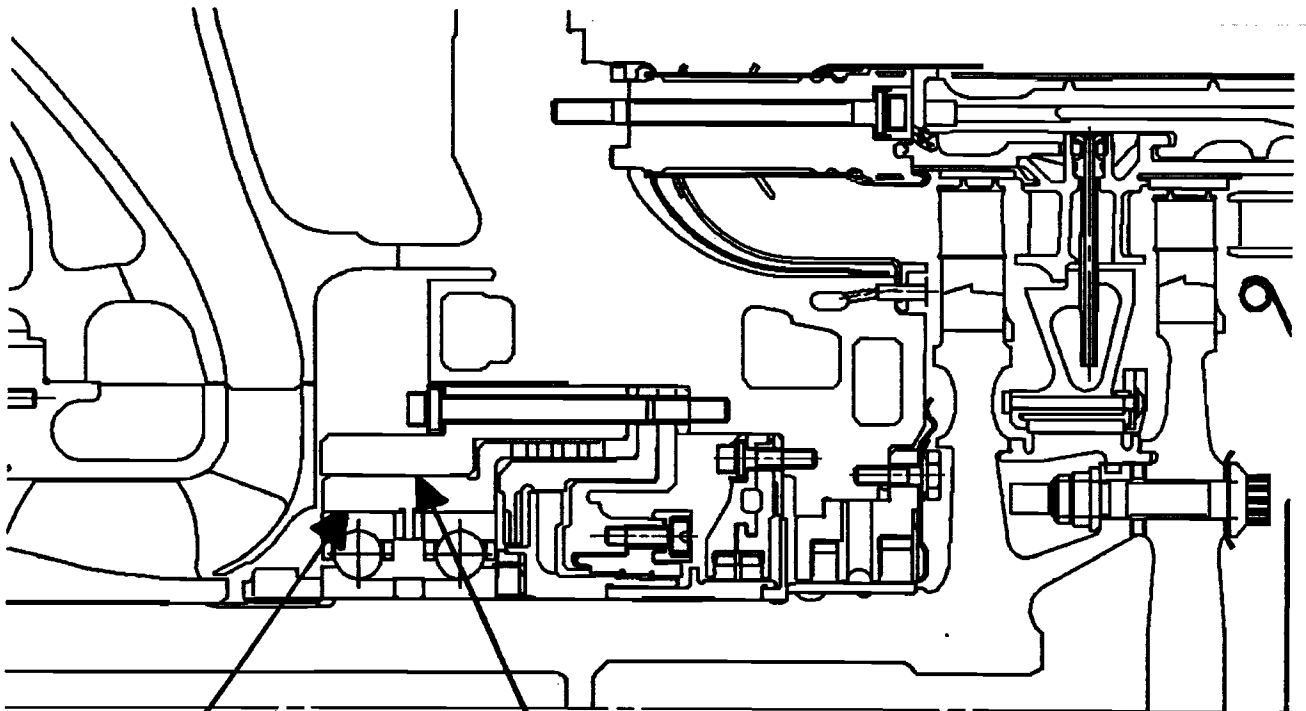

Figure 2. SSME HPOTP Turbine Bearing Package

TABLE 1: NOMINAL BLOCK I HPOTP ROTORDYNAMIC CHARACTERISTICS

MODE	CRITICAL SPEED 1st	CRITICAL SPEED 2nd	SEPARATION MARGIN 2nd Critical to Operating Speed	LOG DEC @ FPL 1st	LOG DEC @ FPL 2nd	STABILITY THRESHOLD SPEED 1st	STABILITY THRESHOLD SPEED 2nd	FIRST MODE FREQ. / OPERATING SPEED
BLOCK I HPOTP	12,128	35,162	14.7 %	0.088	0.085	49,980	45,417	52.2 %

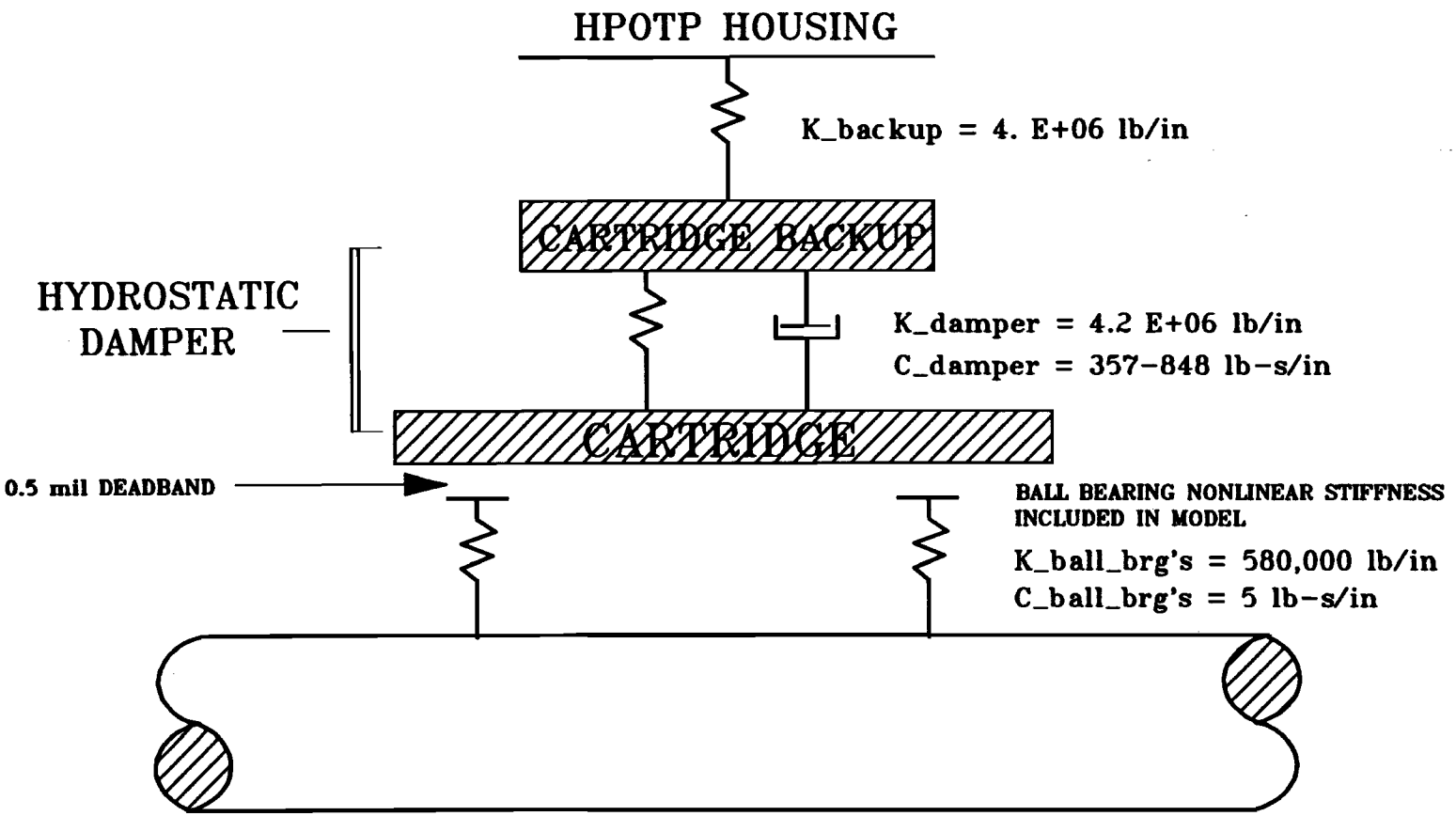

Figure 3. Turbine Bearing Package Nonlinear Model

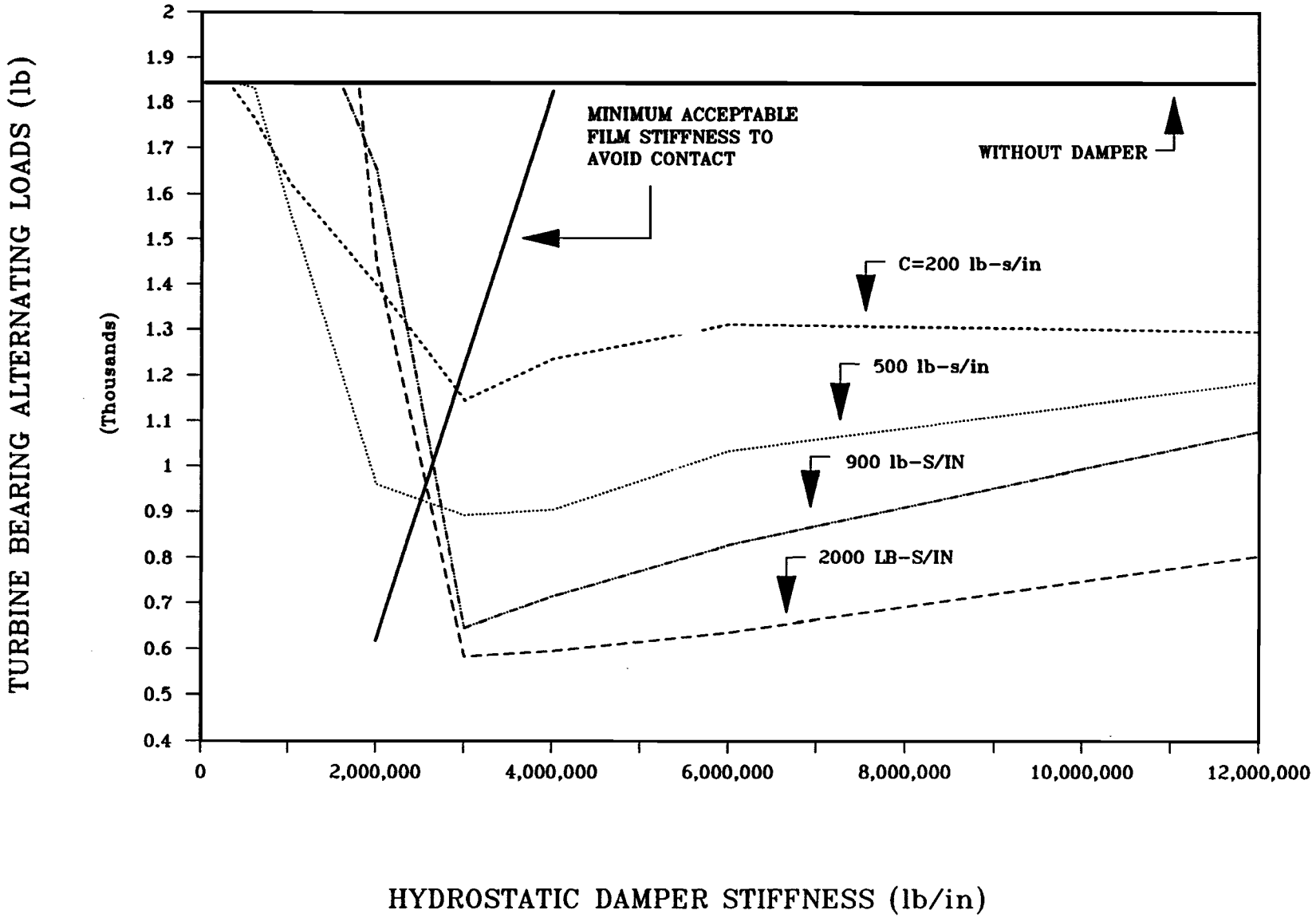

Figure 4. Turbine Bearing Dynamic Load vs. Hydrostatic Damper Characteristics

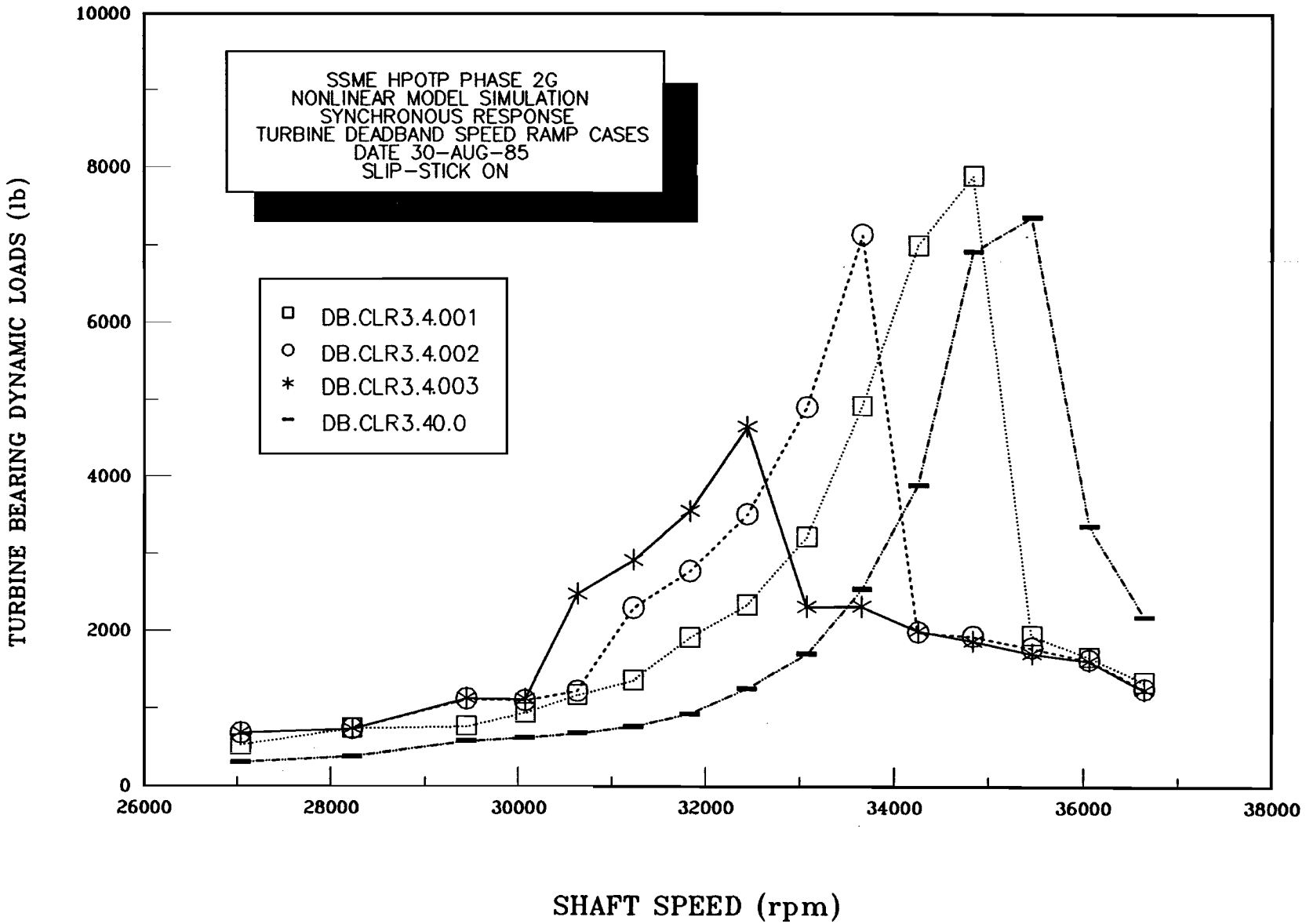

Figure 5. Effect of Cartridge - Backup Support Radial Clearance on Rotor Response

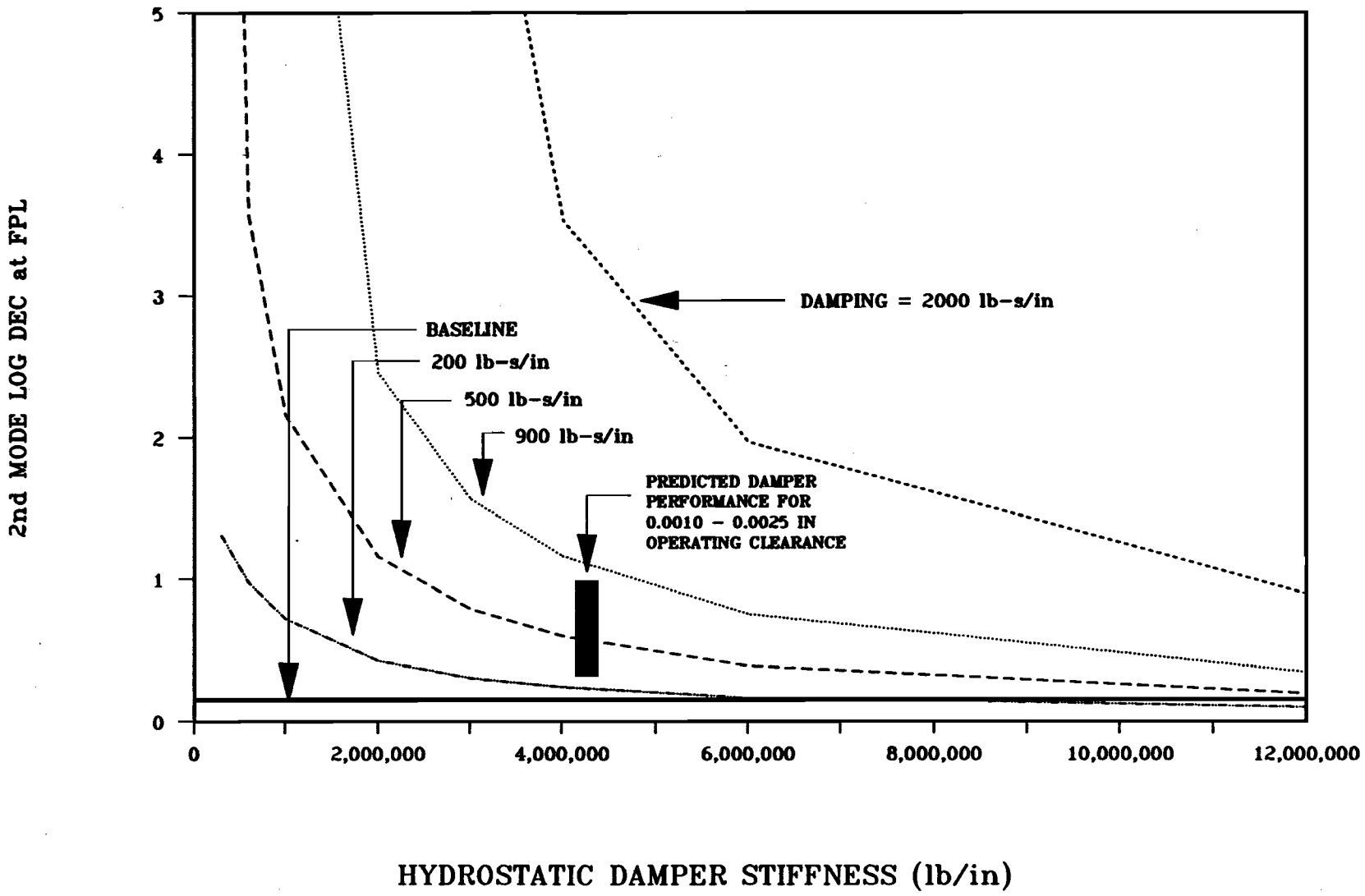

Figure 6. 2nd Rotor Mode Logarithmic Decrement at FPL

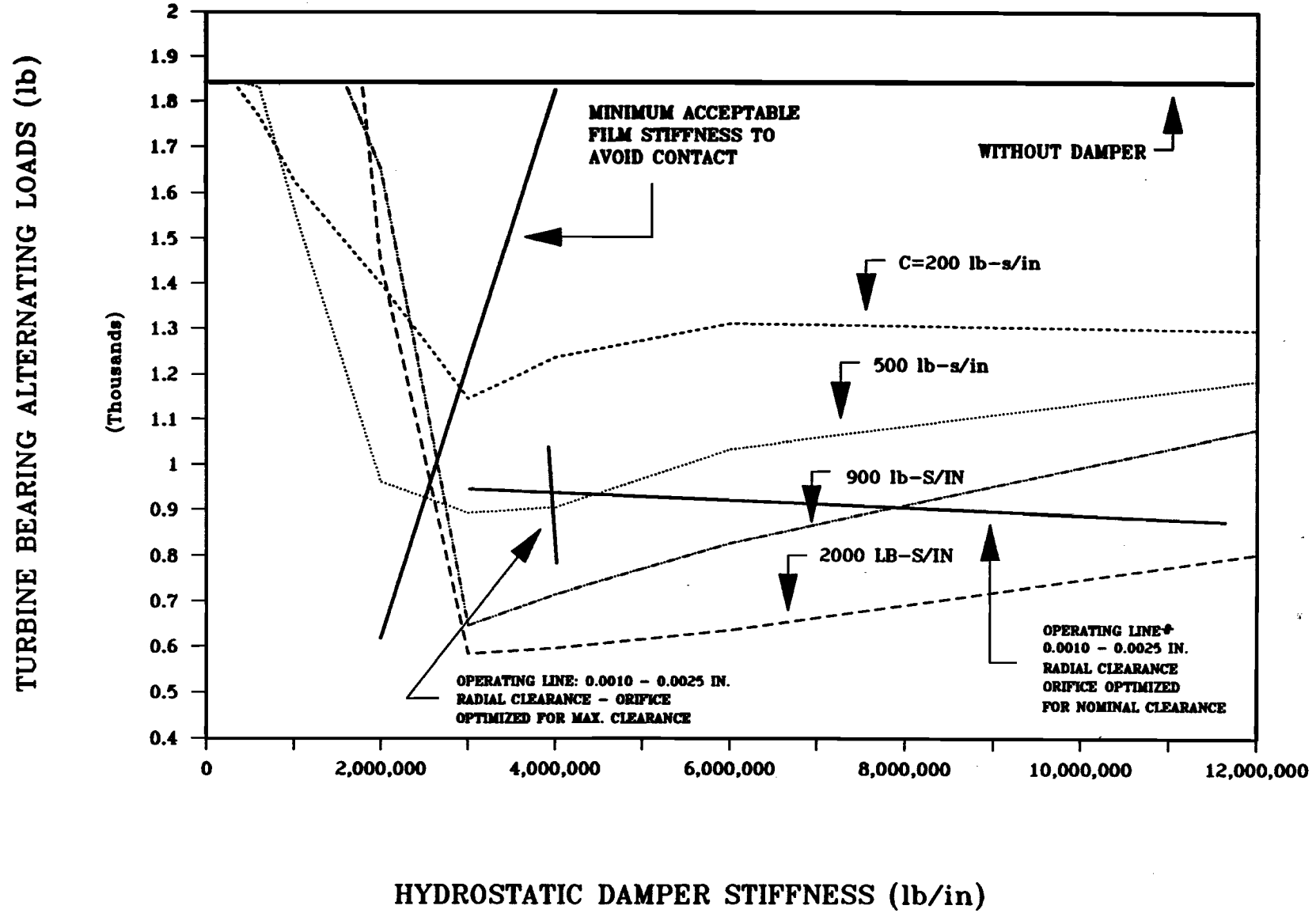

Figure 7. Typical Hydrostatic Damper Performance - Effect of Orifice Optimization

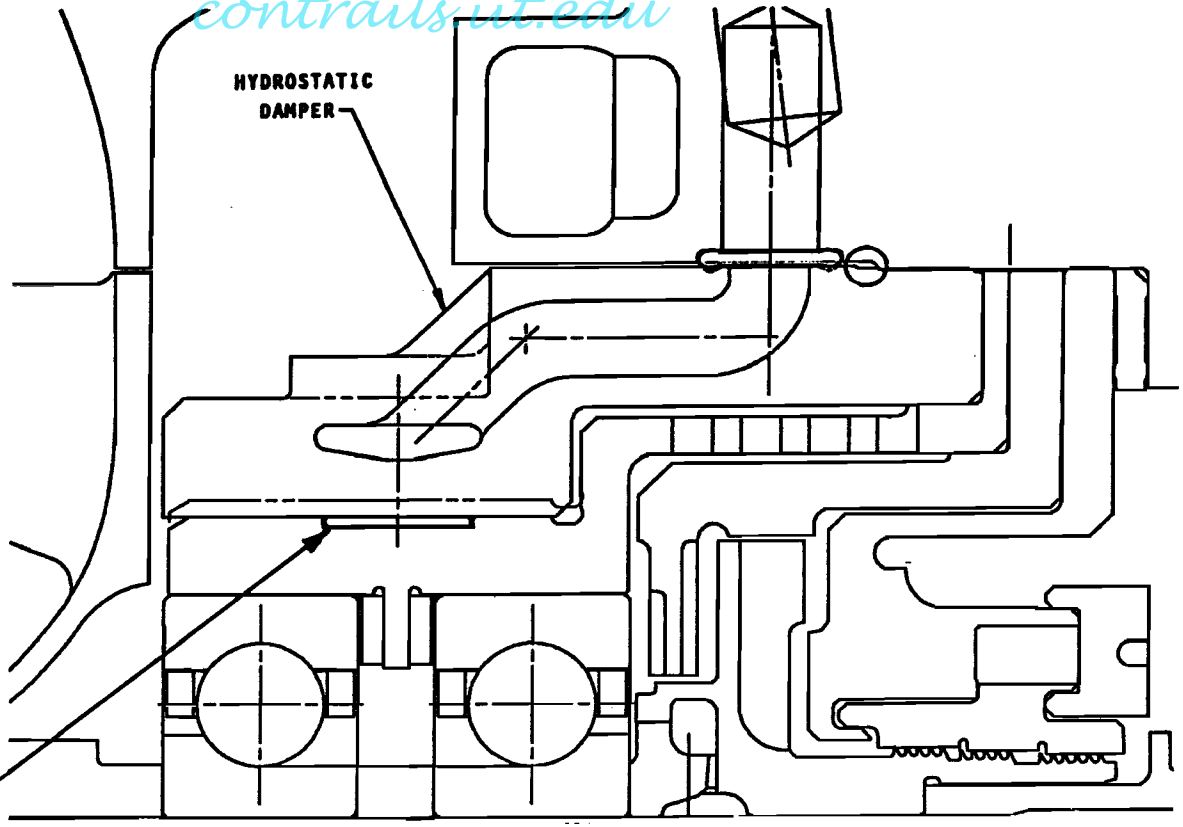

- RECESSES ARE ON CARTRIDGE
  - *NUMBER OF RECESSES = 9*
  - *RECESS DIMENSIONS = 0.457 x 0.914 in.*
  - *RECESS DEPTH = 0.009 - 0.011 in.*
  - *RADIAL CLEARANCE = 0.0010 - 0.0025 in.*
  - *DAMPER LENGTH = 1.25 in. DAMPER DIAMETER = 4.8 in.*

Figure 8. HPOTP Hydrostatic Damper

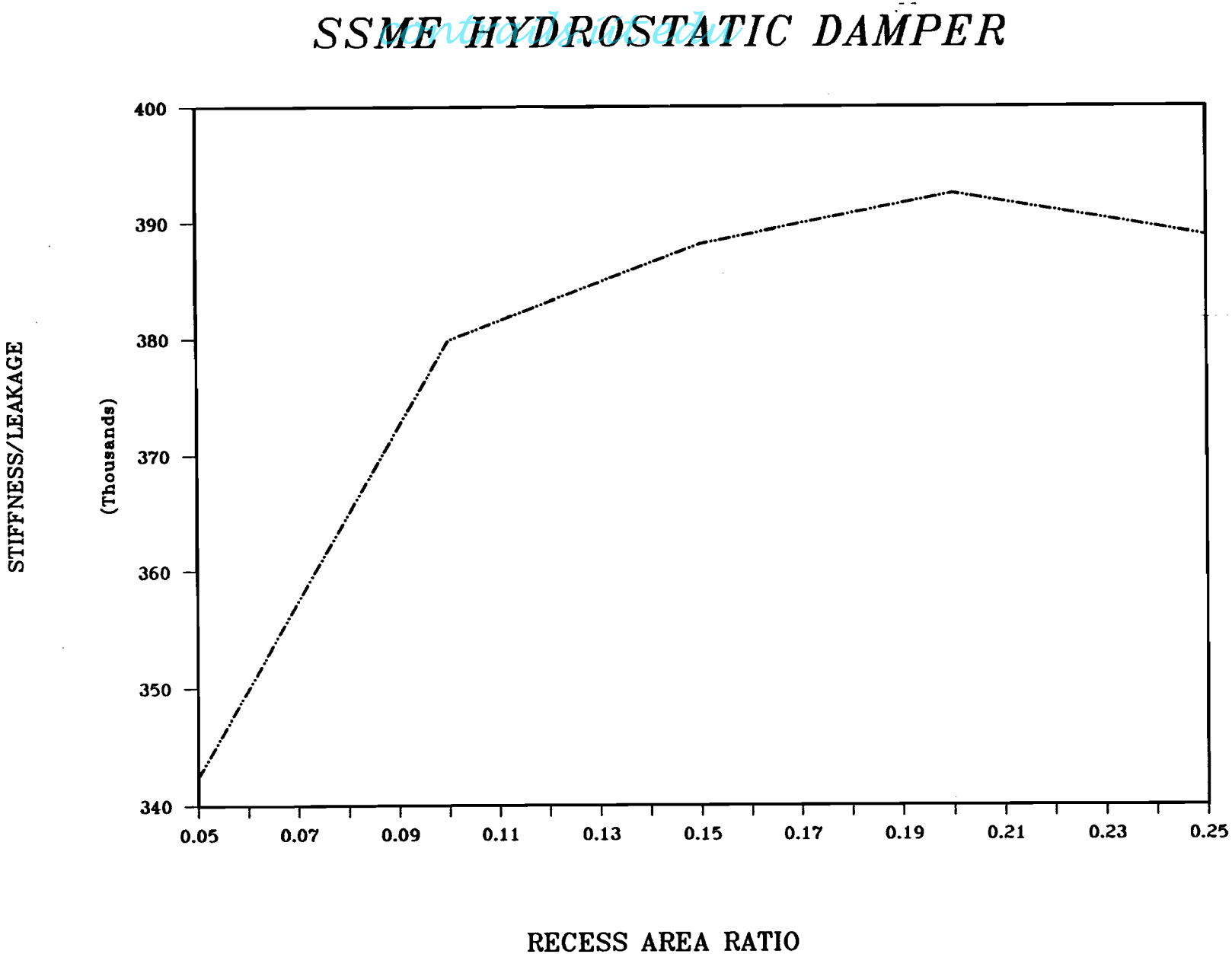

Figure 9. Hydrostatic Damper Stiffness/Leakage Ratio vs. Recess Area Ratio

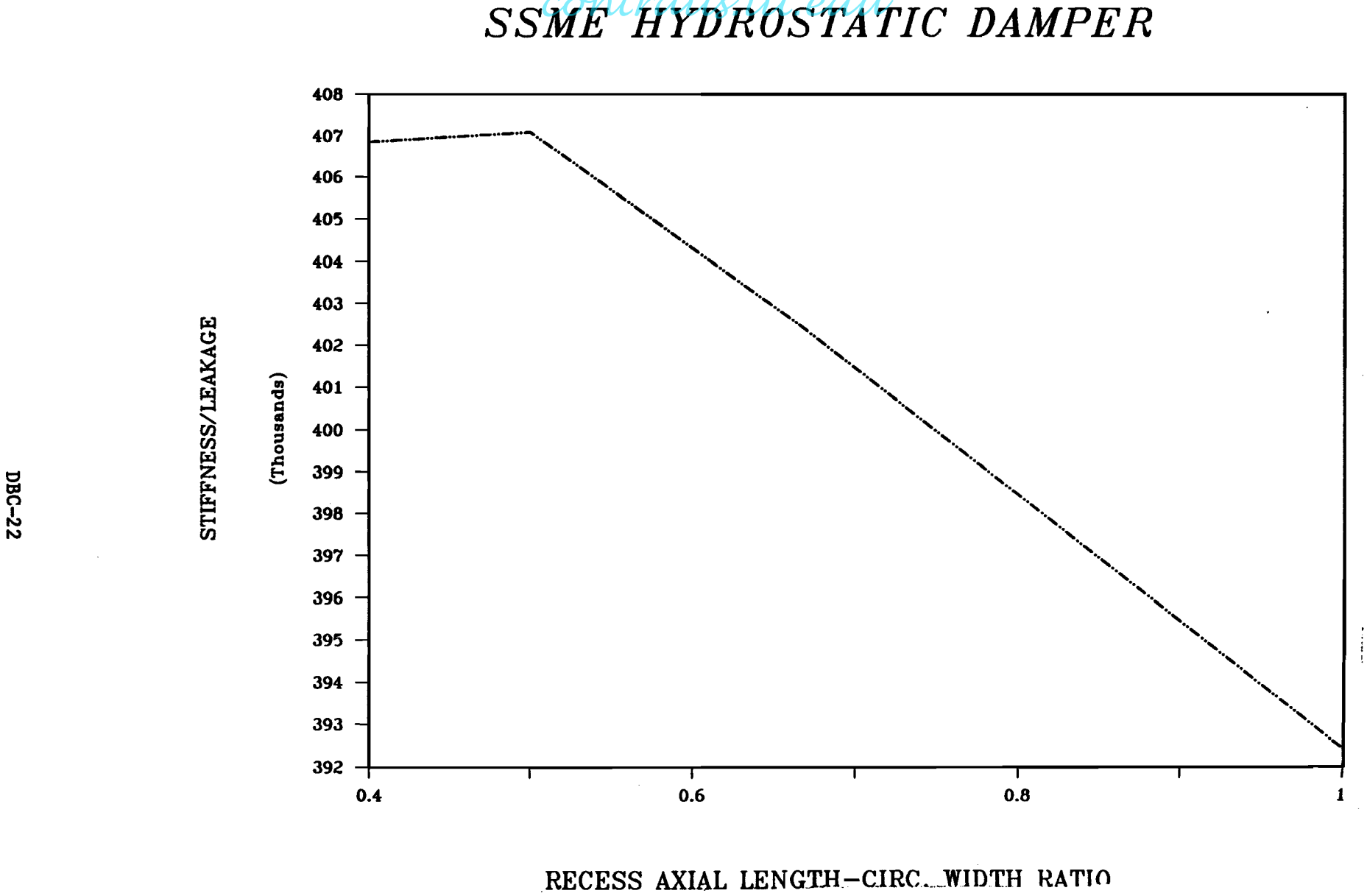

DBC-22

Figure 10. Stiffness/Leakage Ratio Recess vs. Recess Axial Length/Circumferential Width Ratio

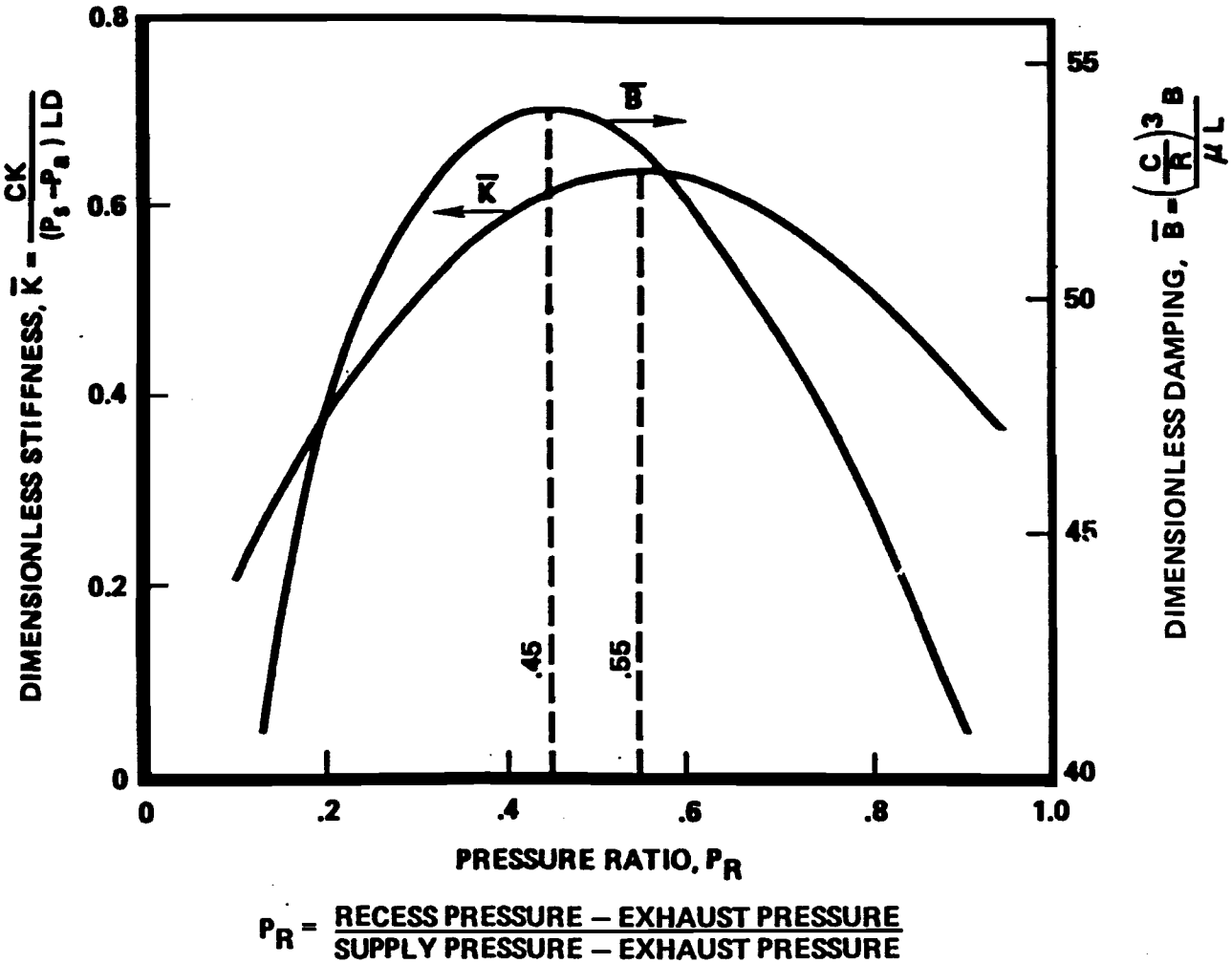

Figure 11. Orifice Diameter Optimization

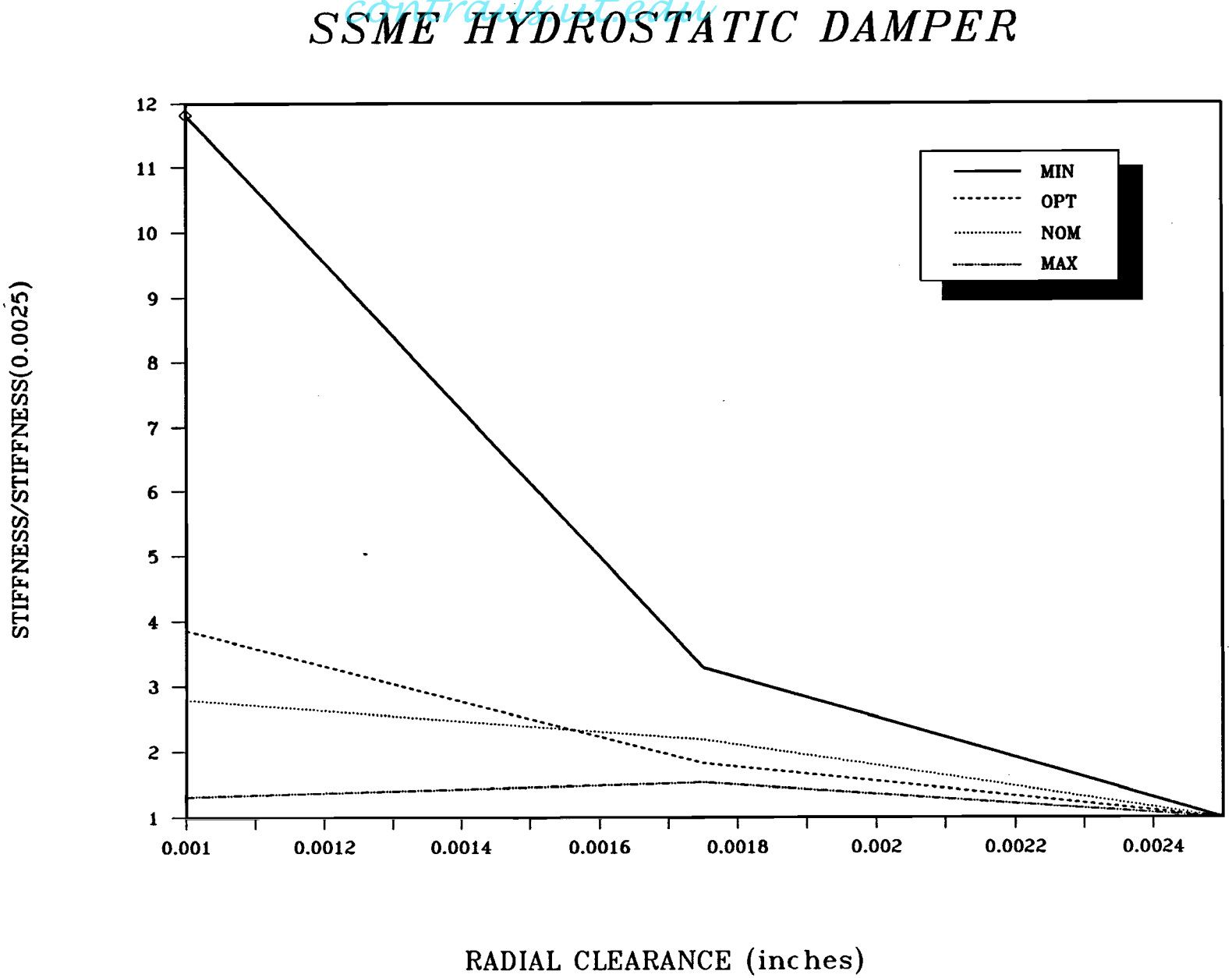

Figure 12. Hydrostatic Damper Stiffness vs. Radial Clearance

TABLE 2: EFFECT OF HYDROSTATIC DAMPER ON LINEAR CRITICAL SPEED AND STABILITY ANALYSIS

MODE	CRITICAL SPEED 1st	CRITICAL SPEED 2nd	SEPARATION MARGIN 2nd Critical to Operating Speed	LOG DEC @ FPL 1st	LOG DEC @ FPL 2nd	STABILITY THRESHOLD SPEED 1st	STABILITY THRESHOLD SPEED 2nd	FIRST MODE FREQ. / OPERATING SPEED
BLOCK I HPOTP	12,128	35,162	14.7 %	0.088	0.085	49,980	45,417	52.2 %
WITH HYDRO-STATIC DAMPER	8,900 −26%	34,950 − 6%	14.1%	0.2 TO 0.33	0.4 TO 0.95	> 50 K	>50 K	52.0%

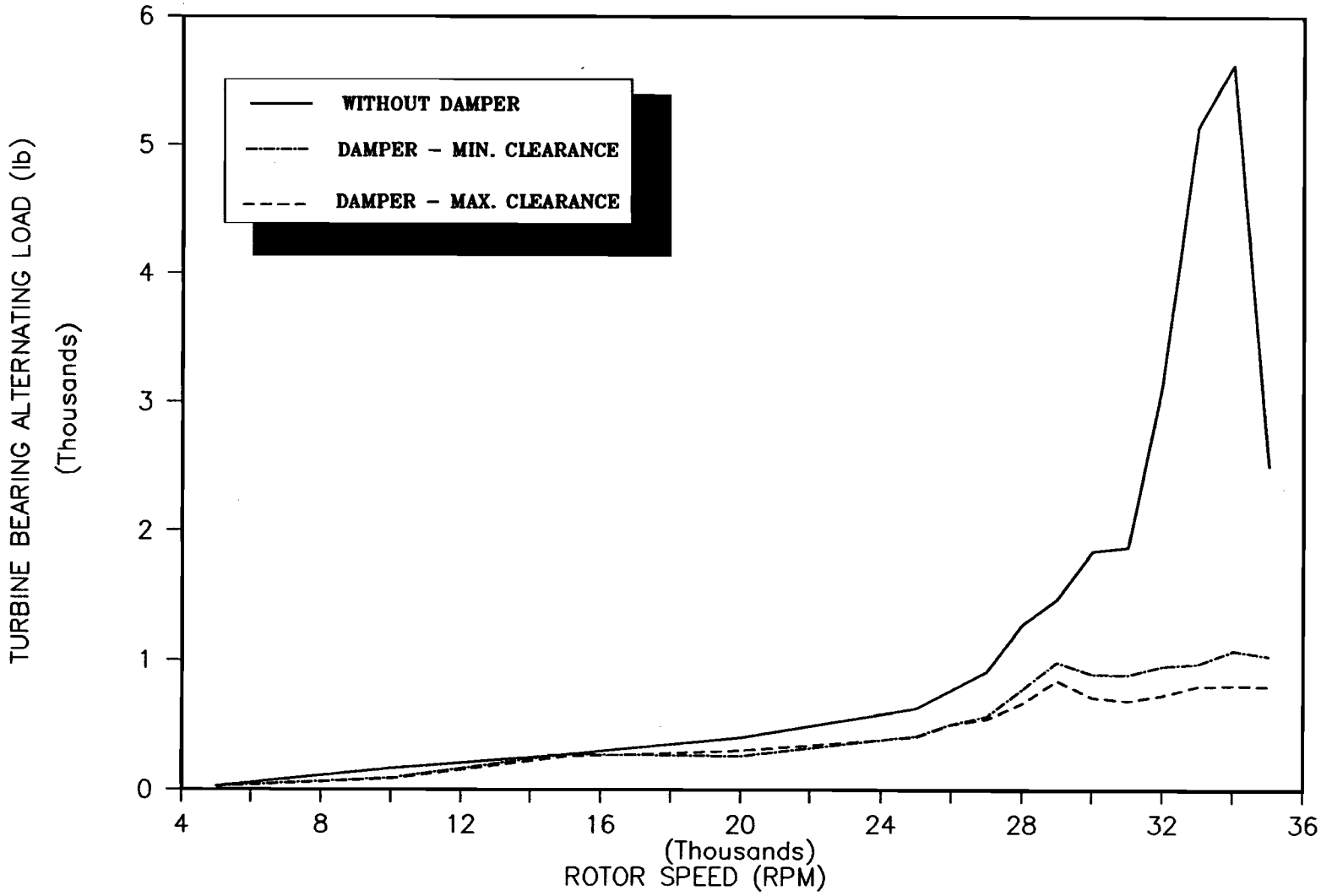

Figure 13. Effect of Hydrostatic Damper on HPOTP Response

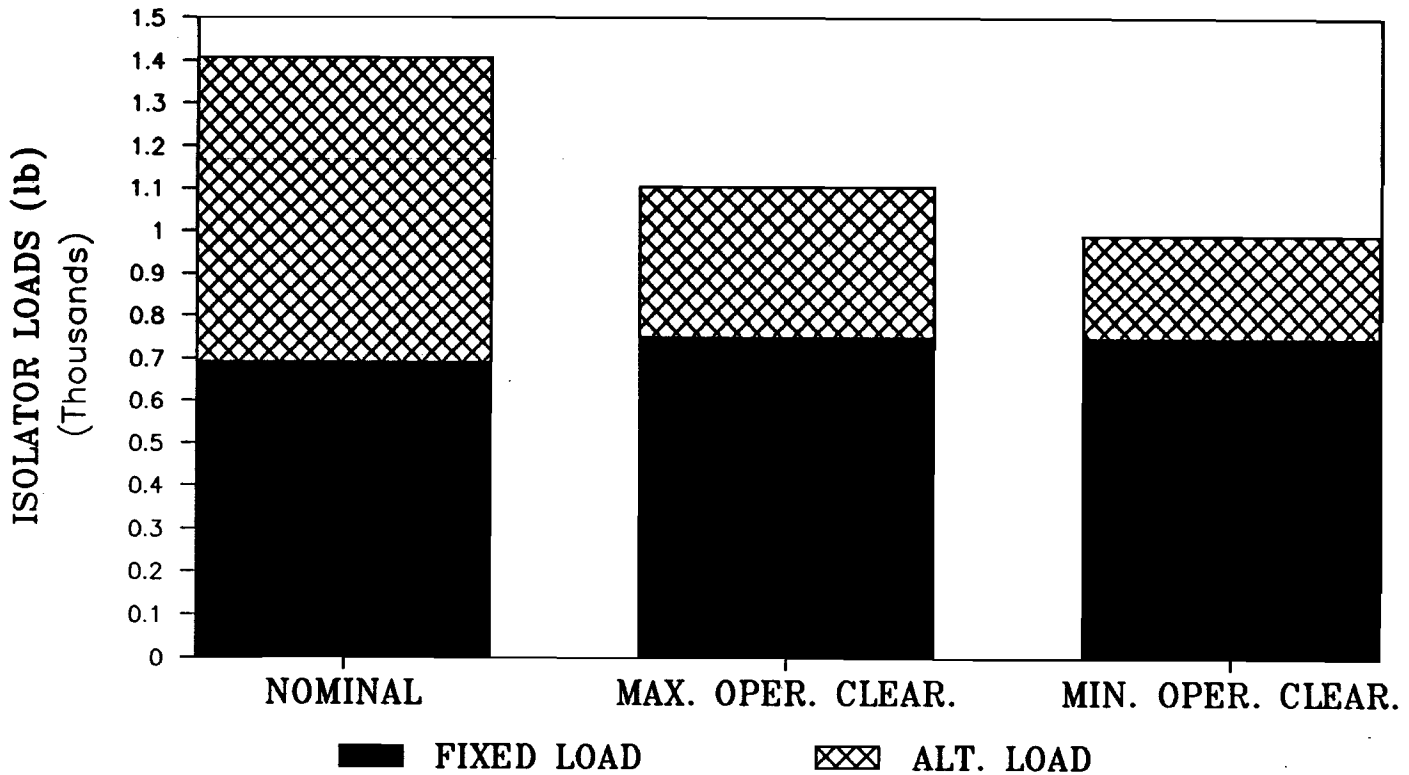

Figure 14. Effect of Hydrostatic Damper on Pump End Bearing Loads at FPL

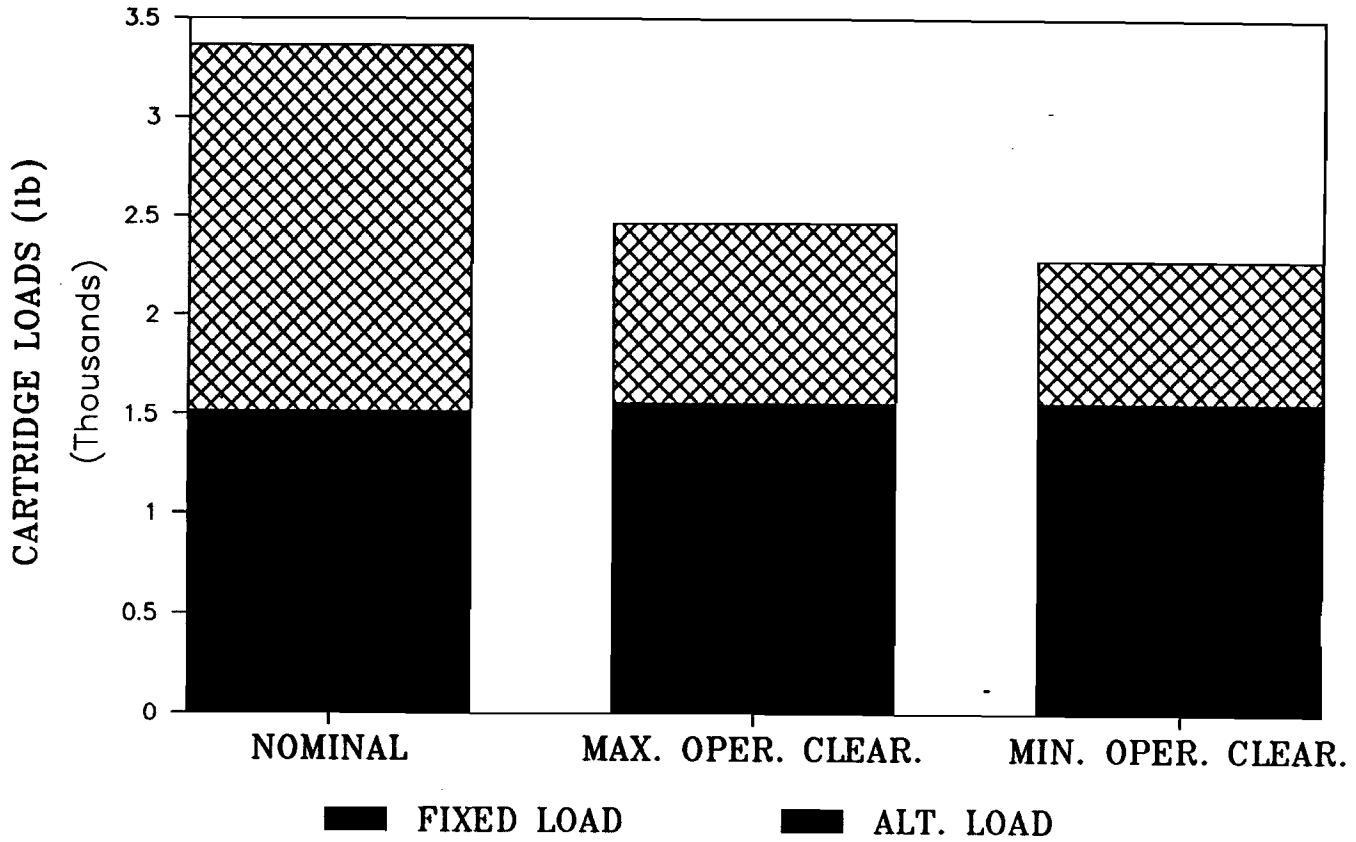

Figure 15. Effect of Hydrostatic Damper on Turbine Bearing Loads at FPL